Numerical Simulation of the Current−Voltage Curve in Dye-Sensitized Solar Cells

Julio Villanueva,[†] Juan A. Anta,*[,‡] Elena Guillén,[‡] and Gerko Oskam*[,†]

Departamento de Física Aplicada, CINVESTAV-IPN, Mérida, Yucatán, México, and Área de Química Física, Universidad Pablo de Olavide, Sevilla, Spain

Received: July 23, 2009; Revised Manuscript Received: September 10, 2009

A theoretical model based on the numerical integration of the continuity equation for electrons with trap-limited density-dependent diffusion and recombination constants is implemented to describe the functioning of dye-sensitized solar cells (DSSC). The application of the model combines recent theory on charge transport in nanocrystalline materials with parameters extracted from five simple measurements: the UV/vis spectrum of the dye in solution, the steady-state current−voltage curve, the open circuit photovoltage versus light intensity curve, photocurrent transient upon switching on an illumination source, and open-circuit voltage decay upon switching off the illumination source. As a novel feature not previously included in this kind of calculations, the model includes an additional term that accounts for the charge transfer from the transparent conducting oxide (TCO) substrate to the electrolyte solution. The general applicability of the model is illustrated by applying it to two different types of cell: a TiO_2-based solar cell with an organic solvent electrolyte and a ZnO-based solar cell with a solvent-free electrolyte. It is found that the numerical model is capable of adequately fitting all data for both systems, resulting in quantitative estimates for the main parameters controlling solar cell functioning and efficiency. The results show that it is possible to provide a global description of DSSCs based on fundamental theories for trap-limited transport and recombination using simple experimental techniques available to every solar cell laboratory. The present paper tries to help fill the gap between pure theoreticians and experimentalists working on this kind of system.

Introduction

Numerical modeling of solar cells is a powerful tool to rationalize and understand the fundamentals of the photoconversion process and to help achieve better performing devices. Since their advent in 1991,[1] solar cells based on sensitized nanostructured, mesoporous metal oxides (dye-sensitized solar cells: DSSCs) are among the most promising third generation devices. DSSCs yield good photoconversion efficiencies, with values of up to 11.1% under 1 sun, AM1.5G illumination.[2,3] In addition, because of the low cost of materials and the simplicity of the fabrication process they offer an inexpensive alternative to conventional silicon-based solar cells.

The performance of DSSCs is based on the combination of good visible light harvesting, efficient charge separation, relatively fast transport, and slow recombination. This fortunate combination is achieved in a system by interpenetrating an electron-conducting material with a "hole-conducting" medium on the nanoscale. In typical DSSCs[4] the electron-conducting material is a mesoporous semiconductor oxide such as TiO_2 or ZnO whereas ion transport in the electrolyte solution provides the charge transport in the second phase. Efficient light harvesting in the visible range is achieved by adsorbing a suitable dye at the metal oxide surface.[5,6] Much of the current research on DSSCs involves developing new hybrid[3,7] and organic dyes[8,9] or improving the optical design of the devices.[10,11] The use of ordered structures for the semiconductor oxide such as nanorods,[12] nanowires,[13] or nanotubes[14] has also been explored in order to accelerate transport. Recent developments[15−17] involve the use of nonvolatile room temperature ionic liquids as the second phase with the aim of achieving stable devices under long-term illumination. Although sometimes ignored, a crucial component of every DSSC device is a transparent conducting oxide (TCO) deposited on a glass substrate that acts as a physical support for the device; even at optimal transparency and conductivity, the TCO introduces series and shunt resistances that might deteriorate the efficiency of the device. Further optimization of DSSCs requires a better insight into the interrelated processes of transport and accumulation of electrons in the mesoporous oxide phase and recombination of electrons with electron acceptors. A physical model based on assumptions related to the fundamental processes taking place in the cell that can adequately describe the solar cell performance is an essential tool in the optimization procedure.

Modeling of DSSCs is an open and active issue[18,19] that involves considerations regarding charge transport and recombination[20−24] as well as light harvesting and interfacial kinetics.[25−27] Electron transport is a key step in the overall cell performance, and it is strongly connected with the issue of recombination. The dynamic competition between electron transport and recombination determines the electron diffusion length.[18,28,29] To achieve good quantum efficiencies under short circuit conditions, the electron diffusion length should be larger than the thickness of the metal oxide film. Electron transport in mesoporous oxide films impregnated with a highly concentrated electrolyte is believed to occur mainly by diffusion.[30,31] Diffusion exhibits anomalous features such as extremely slow transport when compared with compact crystalline materials and diffusion coefficients that depend strongly on light intensity.[32,33] These anomalous features can be explained by the effect of electron traps[34−38] which are thought to correspond to intraband localized states.[37] The presence of the electron traps results in values for the conductivity and the diffusion coefficient of several orders

* To whom correspondence should be addressed.
[†] CINVESTAV-IPN.
[‡] Universidad Pablo de Olavide.

10.1021/jp907011z CCC: $40.75
Published on Web 10/16/2009

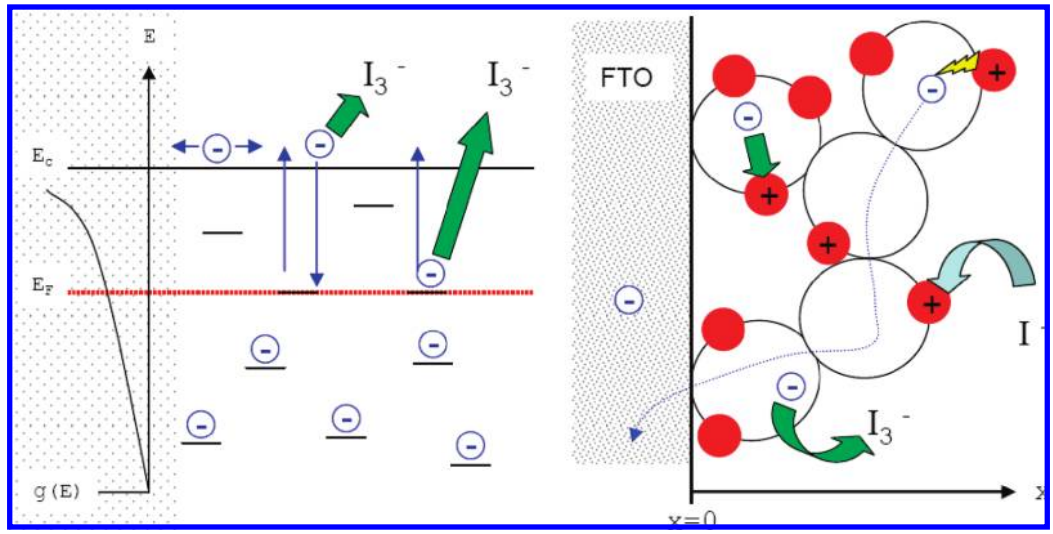

Figure 1. Illustration of the multiple-trapping model of transport (left) and the geometry used to solve the continuity equation (right). In the multiple-trapping model electron transport is assumed to occur via an extended state E_c, but it is slowed down by trapping and detrapping events to and from localized states (shown as thin arrows) with energies distributed along a certain density of states g(E). This mechanism results in an effective diffusion coefficient that depends on the Fermi energy E_F or on the electron density. The continuity equation considered in this paper takes into account such a density-dependent diffusion coefficient to obtain an electron density profile along the x-direction. In addition, recombination processes between electrons and tri-iodide ions and dye cations can occur in the cell under operation (shown as thick arrows). In the present numerical model, the recombination kinetic constant for this process is assumed to also be density-dependent with the same power exponent as the diffusion coefficient. Appropriate boundary conditions are imposed at $x = 0$ for each value of the applied voltage (Fermi energy) so that the full IV (current−voltage) curve can be computed.

of magnitude lower than values obtained in the corresponding bulk, crystalline materials. Moreover, the progressive filling of the traps (as a consequence of increased illumination or applied bias) leads to electron density-dependent transport coefficients. The most widely accepted model that gives rise to these features is the multiple-trapping model.[39−41] In this model, transport is assumed to occur via extended states combined with a succession of trapping and detrapping events in localized states. The multiple-trapping model is related to the quasistatic approximation of Bisquert and Vikhrenko,[40] in which it is assumed that the trapping−detrapping process is much faster than the characteristic time constants for transport and recombination. This fact implies that the relative populations of trapped and free electrons remain at a common equilibrium under small perturbations of the initial state. Both the multiple-trapping model and the quasi-static approximation lead to theoretical expressions to describe electron diffusion[42] and electron recombination.[43] Combination of both models leads to a compensation effect that results in electron diffusion length being a constant when the total electron density is varied.

The widespread use of numerical models for DSSCs has been hindered by the difficulty of finding appropriate fitting parameters or by the complexity of the formalism. Experimental data are usually reported with little connection to theoretical models whereas numerical simulations rely on adjustable parameters that are fitted ad hoc to reproduce very specific measurements. This situation is originated by the intricacy of the experimental system studied, which involves the interaction of very different materials whose properties normally depend on the preparation procedure. Furthermore, the experimental determination of parameters required for the most accepted models, such as the conduction band electron diffusion coefficient or the total trap density, is not straightforward and depends again on the actual characteristics of the utilized materials.

The purpose of this paper is to fill the gap between theoreticians and experimentalists and to propose a simple model that can be easily applied in combination with standard experimental techniques, normally used in solar cell characterization. The model is based on widely accepted theories such as the multiple-trapping formalism and incorporates a simple model for electron recombination, assuming that the recombination rate has the same density-dependence as the diffusion coefficient. We show that under these assumptions, the same results are obtained as those derived from the quasi-static approximation.[43] The model includes an additional term that accounts for the charge transfer from the TCO substrate to the electrolyte solution, which results in an important recombination current at low voltages in the absence of a blocking layer,[44,45] and affects the current−voltage curve and the open circuit voltage decays.

We apply the model to two very different types of solar cell in order to illustrate its applicability and to show how from the fitting of the model to the experimental data we can extract parameters such as the characteristic temperature of the trap distribution, the recombination constant at zero voltage, the transfer parameter at the TCO/electrolyte interface, and the concentration of the adsorbed dye or the diffusion length.

It must be noted that modeling based on impedance spectroscopy,[44] and the combination of intensity-modulated photocurrent spectroscopy (IMPS) and intensity-modulated photovoltage spectroscopy (IMVS),[29] also provide powerful methods to extract these parameters and to gain microscopic information about the devices. However, the method presented in this paper utilizes only steady-state measurements and transients, which are more widely available. The equivalence between frequency-dependent methods and transients has been demonstrated recently.[46]

Theory and Numerical Model

Continuity Equation. The physical model utilized in this work is based on the numerical integration of the continuity equation for electrons with appropriate generation, diffusion, and recombination terms as well as adequate boundary conditions. The continuity equation is solved in a linear geometry (see Figure 1), with the x-coordinate being the distance to the

TCO substrate (working electrode). The model assumes that transport occurs by multiple-trapping so that the electron diffusion coefficient is a function of the total electron density. In addition, the kinetics of recombination to electron acceptors such as tri-iodide ions or oxidized dye molecules (see Figure 1) is assumed to be electron density dependent. The model incorporates an additional recombination term that accounts for electron transfer at the TCO/electrolyte solution interface. Based on these considerations, the continuity equation for electrons has the following form,

$$\frac{\partial n(x,t)}{\partial t} = G(x) + \frac{\partial}{\partial x}\left(D(n)\frac{\partial n(x,t)}{\partial x}\right) - k_R(n)(n(x,t) - n_0^0) + \frac{J_{TCO}}{ed} \quad (1)$$

where $n(x,t)$ is the *total* number density of electrons (as a function of the distance to the working electrode and time), $G(x)$ is the generation rate, $D(n)$ is the density-dependent diffusion coefficient, $k_R(n)$ is the recombination rate, e is the elementary charge, d the film thickness, and J_{TCO} is the charge-transfer current density at the TCO/electrolyte interface. The generation term is a position-dependent function that accounts for electrons injected into the system as a consequence of illumination through the working electrode. Electrons are allowed to diffuse toward the working electrode, which behaves as a collecting interface. Details on the numerical procedure utilized to solve the continuity equation can be found in Appendix A.

Electron Density and Trap Distribution. As mentioned above, we solve the continuity equation using the total electron density, which includes both free and trapped electrons. The majority of the electrons are trapped in an exponential distribution of traps[33,47]

$$g(E) = \frac{\alpha N_t}{k_B T}\exp\left(-\frac{\alpha E}{k_B T}\right) \quad (2)$$

where E is the energy of the trap with respect to the conduction band (defined positive), N_t is the total trap density, and α is a parameter that reflects the average energy of the distribution of trap states below the conduction band.

If the zero-temperature approximation to the Fermi−Dirac distribution is assumed, the total electron density corresponds to the integral of the trap distribution between $E = \infty$ and the quasi-Fermi level, E_F. Using the trap distribution in eq 1 we obtain,

$$E_F(x,t) = -\frac{k_B T}{\alpha}\ln\left(\frac{n(x,t)}{N_t}\right) \quad (3)$$

Consequently, the electronic density is a function of the Fermi energy, and we can define the electron density in the dark and at zero bias at the contact, n_0^0, in terms of the corresponding Fermi energy, E_F^0

$$n = N_t \exp(-\alpha E_F/k_B T) \quad (4)$$

$$n_0^0 = N_t \exp(-\alpha E_F^0/k_B T) \quad (5)$$

The photovoltage under illumination is the difference between the reference Fermi level in the dark and the quasi-Fermi level

$$V = -\frac{(E_F - E_F^0)}{e} = \frac{k_B T}{\alpha e}\ln\frac{n_V^0}{n_0^0} \quad (6)$$

Equation 6 allows determination of the bias dependence of the electron density at the TCO contact. This is the condition imposed to apply the boundary condition at the contact as explained in Appendix A.

Using the total electron density instead of the free electron density is especially convenient for numerical manipulation because the variation of the total density with Fermi level is less pronounced than the free electron density (see eqs 4 and 5 and note that $\alpha < 1$). This facilitates the numerical solution of the continuity equation for density-dependent diffusion coefficients.

Diffusion and Recombination. The electron diffusion coefficient, D, in the nanostructured, mesoporous oxide film has been found to depend strongly on the electron density,

$$D(n) = D_{ref} f(n) = D_{ref}\left(\frac{n}{n_{ref}}\right)^{1-\alpha/\alpha} \quad (7)$$

where D_{ref} is the diffusion coefficient at the *reference* density n_{ref}. Henceforth we take $n_{ref} = n_0^0$ and $D_{ref} = D^0$, i.e., we use the density at zero-bias at the contact as the reference density to compute the density-dependent diffusion coefficient.

This density dependence expressed in eq 7 has been derived from theoretical considerations[40] and from random walk simulation.[31,41,48] For $\alpha = 0.5$, eq 7 recovers a linear dependence of the diffusion coefficient on density, as studied by Cao et al.[49]

In the present model, the recombination constant of electrons with oxidized dye molecules or electron acceptors in the electrolyte is also taken to be density dependent. We apply the observation reported in the literature that this constant has the same electron density dependence as the diffusion coefficient[20]

$$k_R = k_R^{ref} f(n) = k_R^{ref}\left(\frac{n}{n_{ref}}\right)^{1-\alpha/\alpha} \quad (8)$$

where k_R^{ref} is the recombination constant at the *reference* density. Again we take $n_{ref} = n_0^0$ and $k_R^{ref} = k_R^0$. The foundations of eq 8 have been thoroughly discussed in the references listed in the bibliography. Hence, an intuitive explanation of eq 8 is based on the assumption that recombination is transport-limited so that k_R should be proportional to the diffusion coefficient[50,51] A more general derivation assumes that recombination is controlled by the position of the Fermi level in the same way as it affects the diffusion coefficient. This is derived in the context of the "quasi-static approximation"[40] that assumes that the trapping−detrapping process is more rapid than the characteristic time constants for diffusion and recombination, so that the same Fermi-level position controls the kinetics of the transport and recombination with the same power exponent in the total electron density.[40] Power-law functionalities for the diffusion coefficient and the recombination constant are normally found in the experiments, as revealed by transient spectroscopies[52] and electrochemical techniques.[53]

The present model includes an extra term corresponding to charge transfer between the TCO substrate and the electrolyte solution. The dependence of this reaction on the applied bias can be described by the Butler−Volmer equation[45]

$$J_{TCO} = J_{TCO}^{0}\left\{\exp\left[\frac{-(1-b)eV}{k_B T}\right] - \exp\left[\frac{beV}{k_B T}\right]\right\} \quad (9)$$

where J_0^{TCO} is the exchange current density, and b is the cathodic transfer coefficient. As shown by Cameron and co-workers,[54] the introduction of a Butler−Volmer term in the continuity equation leads to nonideal behavior of the open-circuit voltage with respect to the logarithm of the light intensity. The suppression of charge transfer through the TCO/electrolyte produces ideal behavior with a slope of 26 mV at room temperature in the semilogarithmic plot of V_{OC} versus light intensity.

One of the advantages of the present numerical model is that it allows for the possibility to assume that recombination would be governed by the electron transfer processes at the nanostructured metal oxide/electrolyte solution interface, also given by the Butler−Volmer equation. In this case, recombination is limited by the interfacial kinetics (transfer-limited) instead of by the trapping/detrapping process inside the mesoporous oxide (transport-limited).[55] If recombination is transfer-limited, the electron density dependence of the recombination constant is also given by a power law but with an exponent equal to b/α with b being the transfer coefficient at the oxide/electrolyte interface. In this case, a linear dependence of the photovoltage versus the logarithm of the light intensity is obtained but with a nonideal slope. The implications of this scenario have been thoroughly studied in ref 55.

Recombination and Open-Circuit Voltage Decay. In a typical open-circuit voltage decay (OCVD) measurement,[56] the light is switched off, and the voltage decay under open-circuit conditions and in the dark are monitored. In this case no electrons are injected into the film apart from those already present and the diffusion term is zero because no macroscopic gradient is substained within the oxide film at open-circuit. Hence, the continuity eq 1 reduces to

$$\frac{\partial n}{\partial t} = -k_R(n)(n(t) - n_0^0) + \frac{J_{TCO}}{ed} \quad (10)$$

At relatively high voltages, $n >> n_0^0$. Hence,

$$k_R(n) - \frac{J_{TCO}}{ed\,n} = -\frac{1}{n}\frac{dn}{dt} \quad (11)$$

Taking into account eq 11 and changing the integration variable to V_{OC} according to eq 6, we find

$$k_R(n) - \frac{J_{TCO}}{ed\,n} = -\frac{e\alpha}{k_B T}\frac{dV_{OC}}{dt} \quad (12)$$

where $k_R(n)$ is given by eq 8. Note that the same density dependence of the recombination constant is maintained at open circuit, even if there is no macroscopic density gradient and transport toward the TCO external contact. It must be born in mind that in the transport-limited interpretation of eq 8 electrons should diffuse to the recombination centers, and this justifies the power-law dependence of the recombination constant, even at open circuit. In the quasistatic interpretation of eq 8 the density dependence of the recombination constant is a consequence of the system to be at equilibrium,[40] and this condition holds also at open circuit.

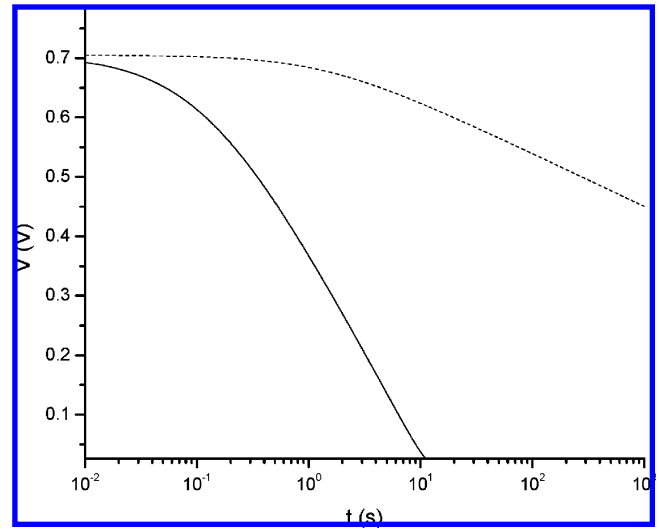

Figure 2. Open-circuit voltage decays as obtained from the solution of eq 12 with (solid line) and without (dashed line) the J_{TCO} term.

Solving eq 12 for V_{OC} we obtain the voltage decay curve at open circuit with two charge-transfer terms, one at the nanostructured oxide surface with kinetics limited by transport, and the other at the TCO layer, with kinetics described by the Butler−Volmer equation. Figure 2 shows the effect of both terms on the open-circuit photovoltage.

Figure 2 shows that the main effect of the charge transfer at the TCO is to accelerate the decay. As reported by Cameron et al.[45] and Peter,[18] this charge loss can be prevented by the use of a blocking layer between the TCO/nanostructured−oxidized interface. In this case, eq 12 can be simplified to the following form

$$k_R(n) = -\frac{e\alpha}{k_B T}\frac{dV_{OC}}{dt} \quad (13)$$

Taking into account eqs 6 and 8, this equation can be solved analytically to obtain,

$$V_{OC} = -\frac{k_B T/e}{1-\alpha}\ln[C_1 + C_2 t] \quad (14)$$

where

$$C_1 = \exp\left(\frac{(\alpha-1)eV_{OC}}{\kappa T}\right);\; C_2 = \frac{k_R^0}{\alpha}(1-\alpha) \quad (15)$$

Equation 15 coincides with the expression found by Walker and co-workers[43] with a derivation based on the quasi-static approximation[40] if we take for the recombination constant at zero voltage

$$k_R^0 = k_{cb}\frac{N_C}{N_t}\left(\frac{n_c^0}{N_C}\right)^{1-\alpha} \quad (16)$$

where k_{cb} is the recombination constant between conduction band electrons and electron acceptors, $n^0{}_c$ is the electron density at the conduction band, and N_c and N_t is the total density of conduction band states and localized states (traps), respectively.

TABLE 1: Summary of the Model Parameters Extracted from Different Experimental Methods

method	measurement	parameter obtained
1	UV/vis spectrum	dye absorption coefficient ($\varepsilon_{sol}(\lambda)$)
2	steady-state current−voltage curve	dye concentration in cell or quantum yield from J_{SC} recombination constant at zero bias, k_R^0, from V_{OC} series resistance R from maximum power point
3	J_{SC}vs time (current rise upon switching on light)	trap distribution parameter, α
4	V_{OC} vs light intensity	electron transfer parameter at TCO interface, b
5	V_{OC} vs time (decay upon switching off light)	+ exchange current density at TCO interface, $J0$TCO

Using the parameters reported by Walker and co-workers[43] ($k_{cb} = 25\ s^{-1}$, $N_c = 10^{21}\ cm^{-3}$, $N_t\ 1.3 \times 10^{18}\ cm^{-3}$, $n_c^0 = 10^4\ cm^{-3}$, $\alpha = T/T_c = 0.35$), we obtain $k_R^0 = 2.7 \times 10^{-7}\ s^{-1}$ from eq 16. Another set of parameters, extracted from the illumination dependence of the photovoltage in nanocrystalline TiO_2, can be found in the literature[26] ($N_c = 4 \times 10^{20}\ cm^{-3}$, $N_t = 2 \times 10^{19}\ cm^{-3}$, $n_c^0 = 8 \times 10^3\ cm^{-3}$). In this case, eq 16 yields $k_R^0 = 3.2 \times 10^{-10}\ s^{-1}$. We will compare these theoretical values with the results of the fittings of the present model with experimental data.

Experimental Procedures and Extraction of Model Parameters

To apply the model presented in the previous section to actual devices and to extract the required parameters, a set of five different experimental measurements should be carried out: (1) UV/vis spectrum of the dye in solution, (2) steady-state photocurrent versus voltage curves at fixed light intensity, (3) photocurrent rise upon switching on an illumination source at fixed light intensity, (4) open circuit photovoltage versus light intensity, and (5) open circuit voltage decay upon switching off the light source. Table 1 shows which parameters can be extracted from each type of measurement.

We have studied two types of solar cell: Cell T, corresponding to a nanostructured, mesoporous TiO_2 cell sensitized with N719 dye and a low-viscosity organic electrolyte solution, and Cell Z, consisting of a nanostructured, mesoporous ZnO cell sensitized with N719 and an ionic liquid electrolyte solution. Details on the experimental procedures are presented in Appendix B.

According to the strategy devised above, the following steps were carried out for the specified cells:

1. The UV/vis spectrum of the N719 dye in ethanol solution at $C_{sol} = 0.16$ mM was obtained. Using the Lambert−Beer law, the absorption coefficient of the dye in solution $\varepsilon_{sol}(\lambda)$ was obtained.

2. The experimental current−voltage curves of the studied cells were obtained at 1 sun illumination. The experimental photocurrent under short circuit conditions was then used to fit the concentration of dye adsorbed in the surface of the oxide C_{dye} by solving the model and using eq A5. For this calculation, we assume that $\phi_{inj} = 1$ for the N719 dye and that the spectrum of the dye is not modified upon adsorption to the oxide surface. Alternatively, the quantum yield can be taken as the adjustable parameter if the concentration of the dye in the cell is known from desorption measurements or can be estimated from the internal surface area of the film.[20] On the other hand, the open circuit photovoltage at 1 sun can be used to obtain a first estimate for the recombination constant k_R^0 via eqs 20 and 21. In this calculation, charge transfer through the TCO/electrolyte interface is initially neglected.

3. The photocurrent rise curve was registered, measuring the photocurrent under short circuit conditions as a function of time upon switching on the illumination at 1 sun. As the numerical model provides $J_{SC}(t)$, these data can be used to obtain the trap distribution parameter α from the best fit to the experimental curve. This calculation is performed assuming that there is recombination under short circuit conditions neither at the oxide interface ($k_R^0 = 0$) nor at the TCO interface ($J_{TCO} = 0$).

4. The photovoltage under open circuit conditions was measured as a function of light intensity between 0.01 and 1 sun. Fitting the data to the numerical model makes it possible to obtain the value of the transfer coefficient b (from the slope of the curve at low illumination) and the exchange current density J_0^{TCO}

5. Knowing the values of C_{dye}, α, J_0^{TCO}, and b, we can obtain a first estimate for k_R^0 by fitting the model results to the experimental value of the open circuit photovoltage V_{OC} at 1 sun.

6. The open circuit voltage decay (OCVD) curve was then measured for the two types of cell starting from the V_{OC} measured at 1 sun. By fitting the experimental data to the theoretical curve derived from eqs 9 and 12, we can refine the estimated values for J_0^{TCO}, and b.

7. Finally the full current−voltage curve is fitted by using and refining all previously obtained parameters and by adjusting the series resistance from the maximum power point.

The following parameters were used for the calculations presented in this paper $n_0^0 = 10^{21}\ m^{-3}$ and $D^0 = 10^{-16}\ m^2\ s^{-1}$. If, for the sake of illustration, we take $E_c - E_{redox} = 1$ eV, $N_t = 10^{25}\ m^{-3}$, $\alpha = 0.2$ (as reported in ref 18), and apply eq 10 where the E_0^F is the redox Fermi level with respect to the conduction band, we can obtain an approximate value of $n_0^0 = 10^{21}\ m^{-3}$. If we consider that under short circuit conditions the quasi-Fermi level is 0.5 eV, $D = 4 \times 10^{-9}\ m^2\ s^{-1}$, and applying eqs 7 and 5, we can obtain the following approximate value of $D^0 = 10^{-16}\ m^2\ s^{-1}$. In addition, a film thickness of $d = 15\ \mu m$ was assumed for the cells.

Results and Discussion

In Supporting Information Figure S1, we show the absorbance spectrum for the N3-dye (similar to the N719 dye) in ethanolic solution at known concentration. This provides the absorption coefficient as a function of wavelength between 350 and 800 nm.

As discussed in the previous section, the short-circuit photocurrent transient was obtained from the model, ignoring all recombination terms. Results compared with the experimental data are shown in Figure 3. As reported in previous work,[20] the

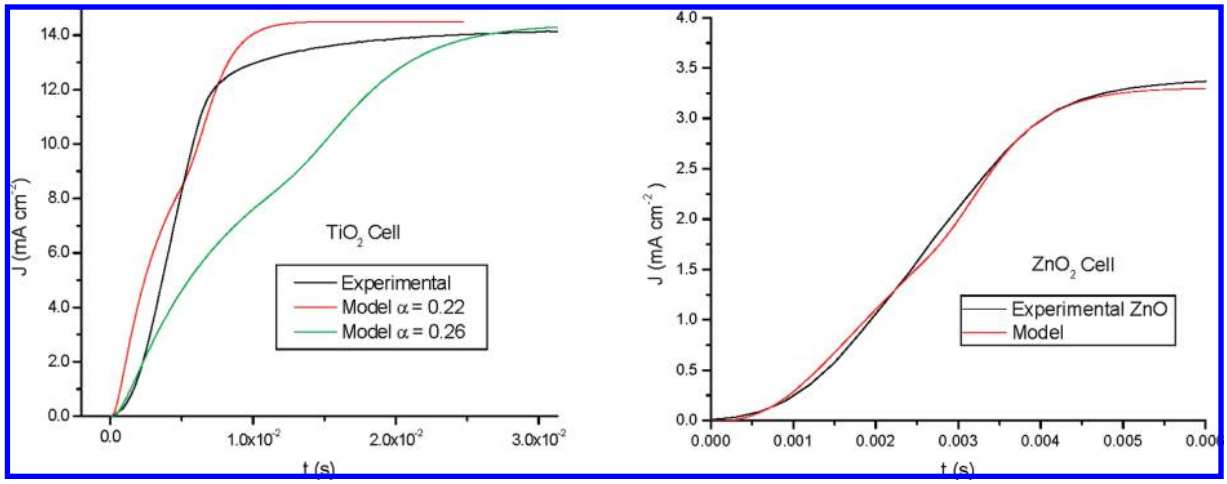

Figure 3. Short-circuit photocurrent transients as obtained from the numerical model without recombination, and experimental data for the two different types of cell. The effect of using different values of α is shown in the left plot.

TABLE 2: Parameters Obtained for the Studied Cells

parameter	Z cell (ZnO)	T cell (TiO_2)
C_{cell} (M)	0.14	0.25
k_R^0 (s^{-1})	9.010^{-7}	3.110^{-9}
α	0.18	0.2
b	0.50	0.55
J_0^{TCO} (A cm^{-2})	1.010^{-4}	1.110^{-5}
R (Ω)	37.5	11.3
L (μm)	10.5	180

adjusted α parameter becomes smaller as the time to reach the stationary state is shorter. This reflects the effect of the density dependence of the diffusion coefficient via eq 12. The steady-state photocurrent at 1 sun is fitted by varying the dye concentration in the numerical solution of the model. The results for α and C_{dye} for both cells can be found in Table 2.

In a similar way, as the experimental steady-state short-circuit photocurrent can be utilized to estimate the light-harvesting characteristics of the cell (via the dye concentration in the present case), the steady-state open-circuit photovoltage at 1 sun is used to obtain a first estimate of the recombination constant k_R^0 from eqs 14 and 15. Here the charge transfer through the TCO/electrolyte interface is initially neglected. The value thus obtained is used to extract the remainder of the parameters from the V_{OC} vs light intensity and V_{OC} vs time experimental data.

Results for the open-circuit photovoltage as a function of light intensity from the numerical model and the experiments can be found in Figure 4. We observe ideal behavior for both cells at high illumination intensity, where the slope of the V_{OC} vs log(light intensity) is close to 26 mV. At low light intensity, the charge transfer through the TCO/electrolyte interface becomes more important.

The numerical results coincide with the findings of Cameron et al.[45] The transfer coefficient that produces the best fit to the experimental data can be obtained from the slope of the curve in the low illumination regime (where charge transfer through the TCO/electrolyte interface is assumed to predominate) with the relation $\theta \cong 26$ mV/b, as predicted by eq 9. It must be noted that a nonideal slope can also occur at high illumination intensity if recombination is transfer-limited as discussed in ref 55. However, this is not the case for the cells studied here, as the photovoltage exhibits a linear dependence with ideal slope at high illumination intensity.

In Figure 5 the voltage decay at switching off the light under open-circuit conditions is reported. The OCVD curves allow determination of the electron transfer current from the TCO to the solution, J_0^{TCO}, and refine the value for b by solving the model at open circuit as stated by eqs 9 and 12. It is observed that the voltage decay is mainly controlled by recombination at the TCO interface; hence, this measurement has a low level of precision

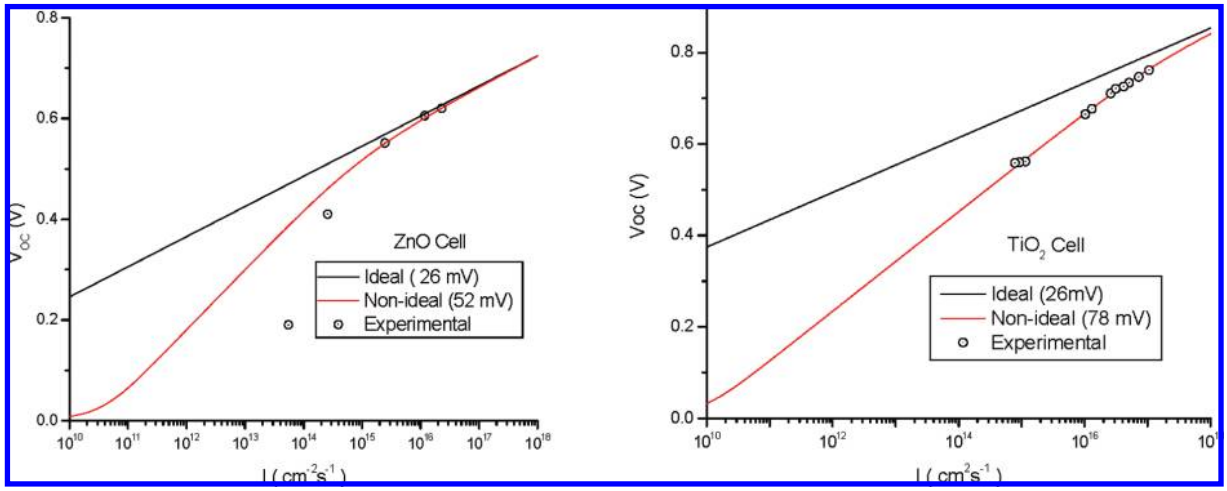

Figure 4. Photovoltage versus light intensity at open circuit as obtained from the experiments and the numerical model.

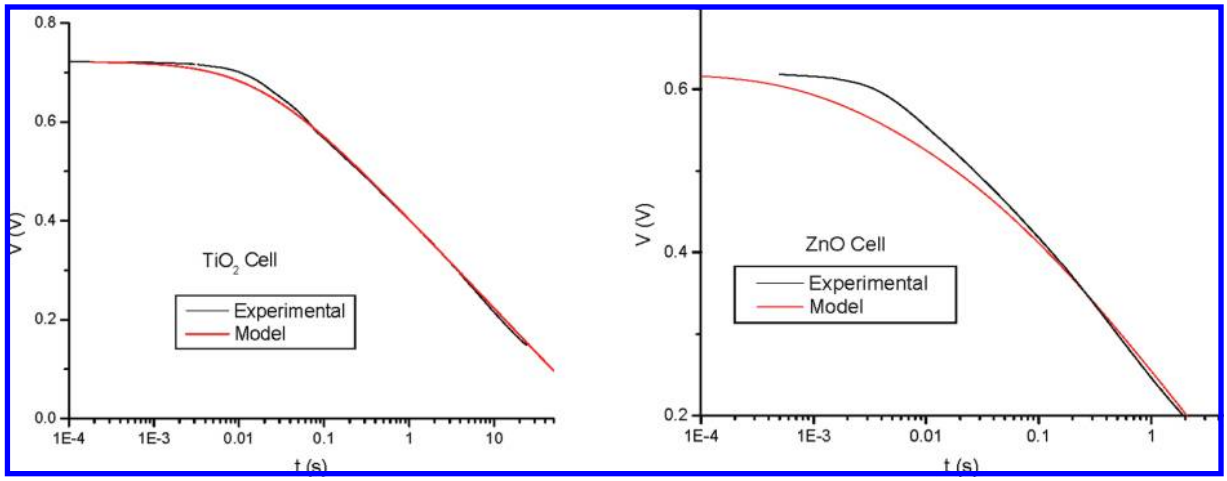

Figure 5. Open-circuit voltage decay as obtained experimentally and best fits from the numerical model as obtained from the solution of eq 12.

for the determination of the recombination characteristics between photoinjected electrons in the nanostructured oxide and the electron acceptors in the electrolyte solution. As noted previously by several authors,[18,43,57] only if an appropriate blocking layer is deposited on the TCO substrate will the OCVD curves reflect recombination from the nanostructured oxide.

Once all light harvesting (ε_{dye}, C_{cell}), diffusion (α), and recombination (k_R^0, b, J_0^{TCO}) parameters are fixed, we can construct the simulated current−voltage plot, as shown in Figure 6. As a final parameter to complete the fitting procedure, the internal series resistance of the cell is incorporated by adjusting the current at maximum power point as described in Appendix A.

A collection of the best fitting parameters for the studied cells are reported in Table 2. We observe that the better performance of cell T with respect to cell Z arises from better light harvesting properties as indicated by a larger dye concentration in the cell, probably due to a larger surface area of the semiconductor film, a lower recombination rate from the semiconductor as indicated from the larger recombination constant for the ZnO cell, and a lower series resistance. The latter parameter is in agreement with expectations, as cells with ionic liquid electrolytes generally exhibit a series resistance larger than that of cells with a low-viscosity organic solvent.[58] In addition, cells based on ionic liquids show strong recombination in comparison with their organic solvent counterparts,[15] which explains the recombination constant of 1 order of magnitude larger for cell Z. The rest of the parameters are similar in both cases and coincide with values previously reported. For instance, an exchange current at the TCO of $j_0 \leq 10^{-4}$ A cm^{-2} has been reported,[26] and transfer coefficients of around 0.5 are common for many reversible redox couples[57]

The electron diffusion length in the present model can be obtained from

$$L = (D_0/k_R^0)^{1/2} \qquad (17)$$

Results found for this are also indicated in Table 2. As expected the diffusion length is of the order of micrometers, as typically found in DSSCs,[18] with larger values found for the best performing cell. It should be noted that when the diffusion length is larger than the film thickness, the electron collection efficiency approaches unity under short circuit conditions, as was derived from the model.

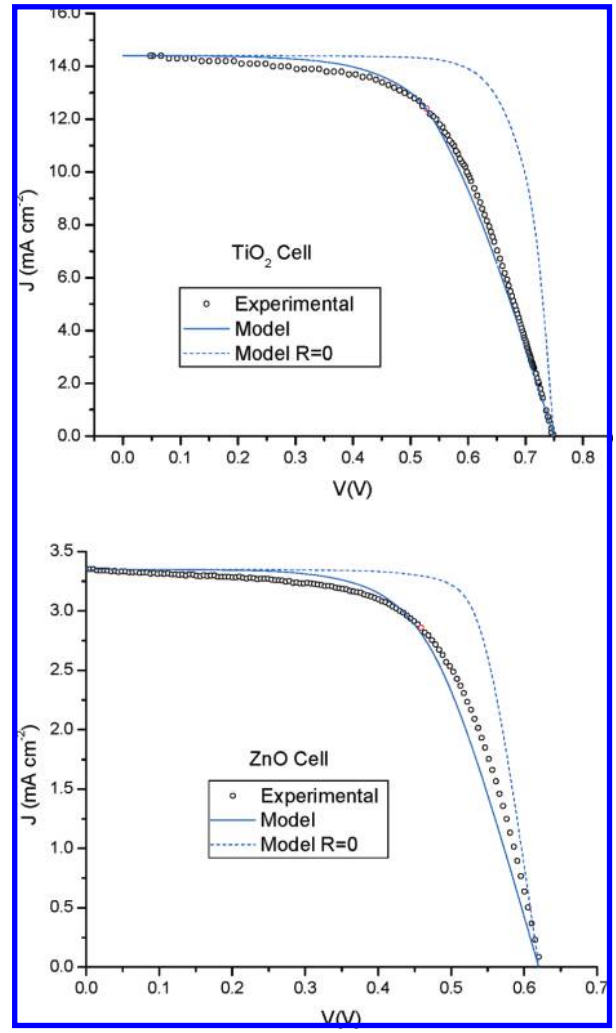

Figure 6. Current−voltage curves for the studied cells. The model data were obtained by solving the continuity eq 1 so that J is computed at different values of the voltage V. The data at finite resistance were obtained from an iterative procedure as described in Appendix A.

Conclusions

In this work, we solve the continuity equation with transport and charge transfer terms in a typical DSSC. The model assumes that diffusion and recombination from the nanostructured oxide depend on the total electron density via a power-law term

consistent with the multiple-trapping model and the quasi-static approximation. As a novel feature not previously included in this kind of calculations, the model includes an additional term that accounts for the charge transfer from the TCO substrate to the electrolyte solution. The model allows calculation of short-circuit photocurrent transients, open circuit photovoltage versus light intensity, open circuit voltage decay curves, and current−voltage curves. By comparing these calculations with experimental data, a set of fitting parameters can be extracted and evaluated.

We have applied the model to two types of cells: a nanostructured TiO_2 mesoporous film and a low-viscosity organic electrolyte solution, and a nanostructured ZnO mesoporous and an ionic liquid electrolyte (solvent-free), both sensitized with N719 dye. When we ignore charge transfer through the FTO/electrolyte interface, the model predicts ideal behavior for the photovoltage−light intensity plot and recovers the theoretical expression for the voltage decay reported previously in the literature.

Our results show that cells without blocking layers can be modeled if appropriate parameters for charge transfer at the TCO/electrolyte interface are introduced. The parameters obtained for the two cells provide a consistent description of the photovoltaic performance of the devices. According to this description and the mechanistic assumptions which were incorporated in the continuity equation, i.e., that recombination has the same power-law dependence as electron diffusion, improving the transport characteristics of the nanostructured oxide film would not imply that the diffusion length and, hence, the efficiency can be increased.

Finally, it is important to stress the relationship between the model proposed here and modeling based on quantum mechanical calculations. These have focused commonly on the computation of the isolated dye and the dye-oxide electronic structure and energy levels.[59,60] These techniques provide a powerful means to derive from first principles the sensitization efficiency of the dye and its quantum injection yield. This information, together with diffusion coefficients obtained from random walk numerical simulation,[61]can be used as input parameters in the numerical model presented here, so that the full IV curve and efficiency can be obtained from first principles for a given dye/oxide/electrolyte combination.

Acknowledgment. This research was supported by CONACYT - México under Grant No. 80002-Y. We thank the Ministerio de Educación y Ciencia of Spain for funding under project HOPE CSD2007-00007 (Consolider-Ingenio 2010), and Junta de Andalucía under projects P06-FQM-01869, P07-FQM-02595 and P07-FQM-02600. E.G. thanks an FPU studentship from Ministerio de Educación y Ciencia of Spain.

Supporting Information Available: Additional information as noted in the text. This material is available free of charge via the Internet at http://pubs.acs.org.

Appendix

Appendix A: Numerical Solution of the Continuity Equation.

Equation 1 is solved by means of the Forward Time Centered Space (FTCS) method using the Lax scheme and with the following boundary conditions:[20]

$$n(x = 0,t) = n_V^0;\ n(x,t = 0) = n_V^0;\ \frac{\partial n(x,t)}{\partial x}_{x=d} = 0 \tag{A1}$$

where n_V^0 is the density at the TCO contact and d the film thickness. These boundary conditions are a consequence of fast electron transfer at the TCO/mesoporous oxide interface. The electron density at contact n_V^0 is an increasing function of the applied bias V, as shown below:

$$n_V^0 = n_0^0 \exp[e\alpha V/k_B T] \tag{A2}$$

with n_0^0 being the density in the dark and at zero bias at the contact, e is the elementary charge, k_B the Boltzmann constant, T the absolute temperature, and α the characteristic parameter of the trap energy distribution (see discussion in the main text).

The numerical solution of eq 1 with boundary conditions A1-A2 gives rise to an electron density profile whose gradient at $x = 0$ ($J_{SC} = (\delta n/\delta x)_{x=0}$) originates the photocurrent. The application of an external bias increases the electron density at the contact and reduces the gradient, so that the photocurrent becomes smaller (see Supporting Information Figure S2). The numerical solution for increasing bias makes it possible to obtain the full current−voltage (IV) curve from the short-circuit situation in which $V = 0$ up to the open-circuit situation for which the photocurrent computed from the electron density gradient is approximately equal to zero.

The generation term $G(x)$ in electrons·m^{-3} s^{-1} is evaluated from

$$G(x) = \int_{\lambda\min}^{\lambda\max} \phi_{inj} I_0(\lambda)\varepsilon_{cell}(\lambda)(1 - R)\ \exp[-\varepsilon_{cell}(\lambda)x]d\lambda \tag{A3}$$

where R is the reflectance (see Note added in Proof), ϕ_{inj} is the electron injection yield and ε_{cell} is the absorption coefficient of the cell (m^{-1}) as a function of wavelength, λ. The incident photon flux $I_0(\lambda)$ (photons m^{-3} s^{-1}) is given by,

$$I_0(\lambda) = \frac{2\pi fc}{\lambda^4}\left[\exp\left[\frac{hc}{\lambda k_B T}\right] - 1\right]^{-1} \tag{A4}$$

where f is a parameter that is adjusted to give the required solar irradiance (see Supporting Information Figure S3).

The absorption coefficient of the cell ε_{cell} can be related to the absorption coefficient of the dye in solution ε_{sol}, by

$$\varepsilon_{cell}(\lambda) = \varepsilon_{sol}(\lambda) \times \frac{C_{dye}(\text{cell})}{C_{dye}(\text{solution})} \tag{A5}$$

where C stands for the concentration of the dye either in solution or when adsorbed at the mesoporous oxide.

To complete the application of the numerical model, a series resistance, R, can be introduced into the calculation.[20] In this case, the voltage V entering eq A2 is replaced by $V = V + JAR$, where J is the current density and A the geometrical surface area. The continuity equation is solved for this new voltage, and the new current obtained is utilized to modify the voltage. The process is repeated until consistency between successive values of J is achieved for a fixed value of R. This consistency

was implemented here by assuming convergence of three significant figures in *J*.

Appendix

Appendix B: Experimental Details.

Cell T was fabricated according to the following procedure: The TiO_2 nanomaterial was prepared using the sol−gel method, from titanium(IV) isopropoxide (Sigma-Aldrich, 97%) and acetic acid (Reasol, 99.7%) in aqueous solution. In a typical synthesis, 15 mL of titanium(IV) isopropoxide was added dropwise to 185 mL of 1 M acetic acid at room temperature with vigorous stirring. The resulting white suspension was peptized at 85 °C in an open erlenmeyer flask with stirring for about 13 h, until a volume of 50 mL remained, corresponding to 80 g L^{-1} TiO_2. The white peptized colloidal dispersion was subsequently treated in a steel autoclave with a Teflon linear (Parr Instruments) at 200 °C for 18 h. After hydrothermal treatment, the colloidal dispersions were sonicated and subsequently further concentrated at 80 °C to a concentration of 130 g L^{-1} TiO_2. PEG 20,000 (Sigma-Aldrich) was added at a concentration of 40 wt.%, and the paste was stirred for 24 h to ensure proper mixing. The solar cell was prepared by consecutively depositing and sintering at 450−500 °C up to three layers using the doctor blading method onto an F-doped SnO_2 (FTO, Hartford Glass, TEC 15) transparent electrode and sensitized with N719 (Solaronix). The electrolyte solution used was Iodolyte AN-50 (Solaronix), and Platisol (Solaronix) was used to prepare a platinized FTO counter electrode.

Cell Z was prepared according to the following procedure: ZnO electrodes deposited on F-doped SnO_2 transparent electrodes were prepared from commercial ZnO powder (Degussa VP AdNanoZnO20) and sensitized with N719 (Solaronix) as explained elsewhere[62,63] The ionic liquid electrolyte was composed of 20% 1-methyl-3-propylimidazolium iodide (PMII, Sigma-Aldrich, > 98%), 80% 1-ethyl-3-methylimidazolium dicyanamide (EMIDCN, Iolitec, >98%), 0.05 M iodine (Sigma-Aldrich, ≥99.5%), 0.1 M lithium iodide (Sigma-Aldrich, 99%), and 1 M *tert*-butylpyridine (TBP, Sigma-Aldrich, 96%).

Except for the determination of the photovoltage as a function of illumination intensity, all measurements were performed at 1 sun (100 mW/cm^2 at room temperature) using a Thermo Oriel Xenon 450 W arc lamp coupled to a water filter and a 325 nm UV blocking filter. A reference solar cell with temperature output (Oriel, 91150) was used for calibration. Light intensity-dependent measurements were performed using neutral density filters. Photocurrents, photovoltages, current−voltage curves, and open-circuit voltage decays were carried out by means of an Autolab/PGSTAT302N station (Ecochemie).

Appendix

Appendix C: Model Parameters.

$n(x,t)$ = total electron density
n_0^0 = electron density defined at zero voltage $n_0^0 = n_{V=0}^0 = n^0(V = 0)$
D^0 = electron coefficient diffusion at zero voltage
α = the average depth of the distribution of the trap states energy
k_R^0 = recombination rate at zero voltage of electron in the conduction band
b = transfer coefficient
e = electron charge
c = speed of light
k_B = Boltzmann constant
T = temperature
j_0^{FTO} = exchange current density transfer
d = thickness of the nanostructured film
ϕ_{inj} = injection coefficient
ε_{cell} = absorption coefficient of the cell
ε_{sol} = absorption coefficient of the dye in solution
A_{sol} = absorbance coefficient of the dye in solution
A_{cell} = absorbance coefficient of the cell
C_{sol} = concentration of dye in solution
C_{cell} = concentration of dye in cell
λ = light wavelength
I_{tot} = total irradiance of light
$I(\lambda)$ = irradiance as a function of the wavelength
J_{SC} = short circuit current
V_{OC} = open circuit voltage
$m=\theta$ = slope in the voltage versus intensity of light curve
R = inner resistance in the cell
N_t = total density of traps in the nanostructured film
E_F = Fermi level
n_c = electron density in the conduction band at a specific Fermi level
n_c^0 = electron density in the dark
N_c = effective density of states in the conduction band
E_F^0 = Fermi level reference
k_c = recombination rate in the quasi-static approximation

Note Added in Proof. Expression A.3 is utilized under the strong assumption that the reflectance of the film is equal to the maximum absorbance at each wavelength so that R = exp(-alfa d). The application of the model with more realistic values of the reflectance would lead to a different value of the dye concentration parameters shown in Table 1.

References and Notes

(1) O'Regan, B.; Grätzel, M. *Nature* **1991**, *353*, 737–740.
(2) Chiba, Y.; Islam, A.; Watanabe, Y.; Komiya, R.; Koide, N.; Han, L. Y. *Jpn. J. Appl. Phys., Part 2* **2006**, *45*, L638–L640.
(3) Gao, F.; Wang, Y.; Shi, D.; Zhang, J.; Wang, M. K.; Jing, X. Y.; Humphry-Baker, R.; Wang, P.; Zakeeruddin, S. M.; Gratzel, M. *J. Am. Chem. Soc.* **2008**, *130*, 10720–10728.
(4) Grätzel, M. *Prog Photovoltaics* **2006**, *14*, 429–442.
(5) Polo, A. S.; Itokazu, M. K.; Iha, N. Y. M. *Coord. Chem. Rev.* **2004**, *248*, 1343–1361.
(6) Robertson, N. *Angew. Chem., Int. Ed.* **2006**, *45*, 2338–2345.
(7) Kuang, D. B.; Klein, C.; Ito, S.; Moser, J. E.; Humphry-Baker, R.; Evans, N.; Duriaux, F.; Graetzel, C.; Zakeeruddin, S. M.; Graetzel, M. *Adv. Mater.* **2007**, *19*, 1133–1137.
(8) Shi, D.; Cao, Y. M.; Pootrakulchote, N.; Yi, Z. H.; Xu, M. F.; Zakeeruddin, S. M.; Graetzel, M.; Wang, P. *J. Phys. Chem. C* **2008**, *112*, 17478–17485.
(9) Caballero, R.; Barea, E. M.; Fabregat-Santiago, F.; de la Cruz, P.; Marquez, L.; Langa, F.; Bisquert, J. *J. Phys. Chem. C* **2008**, *112*, 18623–18627.
(10) Mihi, A.; Calvo, M. E.; Anta, J. A.; Miguez, H. *J. Phys. Chem. C* **2008**, *112*, 13–17.
(11) Hagglund, C.; Zach, M.; Kasemo, B. *Appl. Phys. Lett.* **2008**, 92.
(12) Galoppini, E.; Rochford, J.; Chen, H. H.; Saraf, G.; Lu, Y. C.; Hagfeldt, A.; Boschloo, G. *J. Phys. Chem. B* **2006**, *110*, 16159–16161.
(13) Wu, J. J.; Chen, G. R.; Yang, H. H.; Ku, C. H.; Lai, J. Y. *Appl. Phys. Lett.* **2007**, *90*, 213109.
(14) Zhu, K.; Neale, N. R.; Miedaner, A.; Frank, A. J. *Nano Lett.* **2007**, *7*, 69–74.
(15) Fabregat-Santiago, F.; Bisquert, J.; Palomares, E.; Otero, L.; Kuang, D. B.; Zakeeruddin, S. M.; Grätzel, M. *J. Phys. Chem. C* **2007**, *111*, 6550–6560.
(16) Shi, D.; Pootrakulchote, N.; Li, R. Z.; Guo, J.; Wang, Y.; Zakeeruddin, S. M.; Grätzel, M.; Wang, P. *J. Phys. Chem. C* **2008**, *112*, 17046–17050.
(17) Bai, Y.; Cao, Y. M.; Zhang, J.; Wang, M.; Li, R. Z.; Wang, P.; Zakeeruddin, S. M.; Grätzel, M. *Nat. Mater.* **2008**, *7*, 626–630.
(18) Peter, L. M. *J. Phys. Chem. C* **2007**, *111*, 6601–6612.
(19) Bisquert, J. *Phys. Chem. Chem. Phys.* **2008**, *10*, 49–72.

(20) Anta, J. A.; Casanueva, F.; Oskam, G. *J. Phys. Chem. B* **2006**, *110*, 5372–5378.
(21) Nelson, J.; Chandler, R. E. *Coord. Chem. Rev.* **2004**, *248*, 1181–1194.
(22) Petrozza, A.; Groves, C.; Snaith, H. J. *J. Am. Chem. Soc.* **2008**, *130*, 12912–12920.
(23) Bisquert, J.; Grätzel, M.; Wang, Q.; Fabregat-Santiago, F. *J. Phys. Chem. B* **2006**, *110*, 11284–11290.
(24) Kambili, A.; Walker, A. B.; Qiu, F. L.; Fisher, A. C.; Savin, A. D.; Peter, L. M. *Physica E (Amsterdam, Neth.)* **2002**, *14*, 203–209.
(25) Ferber, J.; Stangl, R.; Luther, J. *Sol. Energy Mater. Sol. Cells* **1998**, *53*, 29–54.
(26) Salvador, P.; Hidalgo, M. G.; Zaban, A.; Bisquert, J. *J. Phys. Chem. B* **2005**, *109*, 15915–15926.
(27) Penny, M.; Farrell, T.; Will, G. *Sol. Energy Mater. Sol. Cells* **2008**, *92*, 24–37.
(28) Peter, L. M.; Wijayantha, K. G. U. *Electrochim. Acta* **2000**, *45*, 4543–4551.
(29) Dunn, H. K.; Peter, L. M. *J. Phys. Chem. C* **2009**, *113*, 4726–4731.
(30) Sodergren, S.; Hagfeldt, A.; Olsson, J.; Lindquist, S. E. *J. Phys. Chem.* **1994**, *98*, 5552–5556.
(31) van de Lagemaat, J.; Frank, A. J. *J. Phys. Chem. B* **2001**, *105*, 11194–11205.
(32) Nelson, J. *Phys. Rev. B* **1999**, *59*, 15374–15380.
(33) Peter, L. M.; Duffy, N. W.; Wang, R. L.; Wijayantha, K. G. U. *J. Electroanal. Chem.* **2002**, *524*, 127–136.
(34) Schmidlin, F. W. *Bull. Am. Phys. Soc.* **1977**, *22*, 346–346.
(35) Silver, M.; Cohen, L. *Phys. Rev. B* **1977**, *15*, 3276–3278.
(36) Solbrand, A.; Henningsson, A.; Sodergren, S.; Lindstrom, H.; Hagfeldt, A.; Lindquist, S. E. *J. Phys. Chem. B* **1999**, *103*, 1078–1083.
(37) Konenkamp, R. *Phys. Rev. B* **2000**, *61*, 11057–11064.
(38) Bailes, M.; Cameron, P. J.; Lobato, K.; Peter, L. M. *J. Phys. Chem. B* **2005**, *109*, 15429–15435.
(39) Tiedje, T.; Rose, A. *Solid State Commun.* **1981**, *37*, 49–52.
(40) Bisquert, J.; Vikhrenko, V. S. *J. Phys. Chem. B* **2004**, *108*, 2313–2322.
(41) Anta, J. A.; Nelson, J.; Quirke, N. *Phys. Rev. B* **2002**, *65*, 125324.
(42) Anta, J. A.; Mora-Sero, I.; Dittrich, T.; Bisquert, J. *Phys. Chem. Chem. Phys.* **2008**, *10*, 4478–4485.
(43) Walker, A. B.; Peter, L. M.; Lobato, K.; Cameron, P. J. *J. Phys. Chem. B* **2006**, *110*, 25504–25507.
(44) Wang, Q.; Ito, S.; Grätzel, M.; Fabregat-Santiago, F.; Mora-Sero, I.; Bisquert, J.; Bessho, T.; Imai, H. *J. Phys. Chem. B* **2006**, *110*, 25210–25221.
(45) Cameron, P. J.; Peter, L. M.; Hore, S. *J. Phys. Chem. B* **2005**, *109*, 930–936.
(46) Wang, M.; Chen, P.; Humphry-Baker, R.; Zakeeruddin, S.; Grätzel, M. *ChemPhysChem* **2009**, *10*, 290–299.
(47) Bisquert, J.; Fabregat-Santiago, F.; Mora-Sero, I.; Garcia-Belmonte, G.; Barea, E. M.; Palomares, E. *Inorg. Chim. Acta* **2008**, *361*, 684–698.
(48) van de Lagemaat, J.; Kopidakis, N.; Neale, N. R.; Frank, A. J. *Phys. Rev. B* **2005**, 71.
(49) Cao, F.; Oskam, G.; Meyer, G. J.; Searson, P. C. *J. Phys. Chem.* **1996**, *100*, 17021–17027.
(50) Nelson, J.; Haque, S. A.; Klug, D. R.; Durrant, J. R. *Phys. Rev. B* **2001**, 6320.
(51) Kopidakis, N.; Benkstein, K. D.; van de Lagemaat, J.; Frank, A. J. *J. Phys. Chem. B* **2003**, *107*, 11307–11315.
(52) Haque, S. A.; Tachibana, Y.; Willis, R. L.; Moser, J. E.; Grätzel, M.; Klug, D. R.; Durrant, J. R. *J. Phys. Chem. B* **2000**, *104*, 538–547.
(53) Peter, L. M.; Wijayantha, K. G. U. *Electrochem. Commun.* **1999**, *1*, 576–580.
(54) Cameron, P. J.; Peter, L. M. *J. Phys. Chem. B* **2005**, *109*, 7392–7398.
(55) Villanueva-Cab, J.; Oskam, G.; Anta, J. Sol. Energy. Mater. Sol. Cells. doi:, 10.1016/j.solmat.2009.06.004.
(56) Bisquert, J.; Zaban, A.; Greenshtein, M.; Mora-Sero, I. *J. Am. Chem. Soc.* **2004**, *126*, 13550–13559.
(57) Cameron, P. J.; Peter, L. M. *J. Phys. Chem. B* **2003**, *107*, 14394–14400.
(58) Kubo, W.; Kambe, S.; Nakade, S.; Kitamura, T.; Hanabusa, K.; Wada, Y.; Yanagida, S. *J. Phys. Chem. B* **2003**, *107*, 4374–4381.
(59) De Angelis, F.; Fantacci, S.; Selloni, A. *Nanotechnology* **2008**, 19.
(60) Duncan, W. R.; Prezhdo, O. V. *J. Am. Chem. Soc.* **2008**, *130*, 9756–9762.
(61) Anta, J. A. *Energy Environ. Sci.* **2009**, *2*, 387–392.
(62) Guillen, E.; Casanueva, F.; Anta, J. A.; Vega-Poot, A.; Oskam, G.; Alcantara, R.; Fernandez-Lorenzo, C.; Martin-Calleja, J. *J. Photochem. Photobiol., A* **2008**, *200*, 364–370.
(63) Guillén, E.; Fernández-Lorenzo, C.; Alcántara, R.; Martín-Calleja, J.; Anta, J. *Sol. Energy Mater. Sol. Cells* **2009**, *93*, 1846–1852.

JP907011Z